DOI: 10.15480/882.9305

Eighth International Symposium on Marine Propulsors
smp'24, Berlin, Germany, March 2024

Reduction of Radiated Propeller Noise of Underwater Vehicles during Acceleration Maneuvers

Moustafa Yasser Moustafa [1], Mohamed Elgohary [2], Moustafa Abdel-Maksoud[3], Mohamed Fathy Fouad[1],Amany Mohamed [4]

[1]Egyptian Armed Forces, Egypt
[2] Borg Al Arab technological university, Alexandria, Egypt
[3]Hamburg University of Technology, Hamburg, Germany
[4] Naval Architecture and Marine Engineering Department Alexandria University, Alexandria, Egypt

ABSTRACT

An acceleration maneuver may have critical operating phases where the propeller is subjected to unsteady flow conditions in addition to gradual or sudden changes in the number of revolutions per second (RPS). In the present study, a control model is developed to assist the acceleration maneuver of underwater vehicles in calm water under various operating conditions, in which the increase in propeller speed is precisely controlled to ensure the avoidance of tip vortex cavitation and to enable a reduction in the non-cavitating noise radiated by the propeller during the acceleration maneuver.

As a test case for the study, the DARPA SUBOFF geometry (Defense Advanced Research Projects Agency) in combination with the CNR-INM E1619 propeller is selected. The numerical simulations are conducted using the RANSE-solver STAR-CCM+. The hybrid method, which combines CFD and P-FWH is applied to calculate the acoustic pressure and estimate the propeller radiated noise.

The provided control model shows that the inception of the tip vortex cavitation can be avoided during the acceleration maneuver. In addition, the noise radiation can be reduced when the control model is activated.

Keywords

Acceleration; P-FWH; Submarine; Propeller- Noise.

1 INTRODUCTION

Mitigating the noise emitted by underwater vehicles reduces the harmful effects on marine life and thus marine pollution. Underwater vehicles usually have many noise sources, such as engines or propulsion systems. Beyond a certain speed, the propeller can be considered to be the main source of the noise radiated by underwater vehicles. The non-uniform wake field caused by the boundary layer on the hull and appendages of the vehicle results in non-uniform loading of the propeller blades. In addition, different environmental conditions such as water depth, temperature and water quality can also play an important role.

The acceleration of underwater vehicles is one of the critical operation phases in which the propeller faces unsteady inflow conditions besides the gradual or sudden change in the number of rotations per second. Therefore, the propeller experiences pressure fluctuations on the blades which increase the potential of non – cavitating and cavitating underwater noise.

For deeply submerged conditions, non-cavitating noise is dominant due to the fluctuating force acting on the blades of the propeller especially, during acceleration when the number of revolutions per second rises and the flow field is accelerated, leading to an increase in turbulence. While in near-surface conditions, pressure may fall under vapor pressure. In this situation, cavitation noise can be the dominant sound source. In reality, different types of cavitation can be experienced, but tip vortex cavitation is considered to be the first type of cavitation that occurs.

According to Franc & Michel (2003), the occurrence of cavitation can be divided into two main stages. Firstly, the inception, which takes place in the stage between non-cavitating and cavitating conditions. The second stage is the fully developed cavitation when the cavity pattern becomes visible. Experimental and numerical analysis of cavitation inception of propellers under open water conditions was conducted by many researchers, Asnaghi et al. (2018a). In addition, the analysis of different tip vortex prediction methods was carried out by Asnaghi et al. (2018b).

The inception of TVC is a complex process, which can be influenced by several factors and whose modelling requires a sophisticated mathematical description. Several researchers have developed models for prediction of TVC inception in model scale and attempted to use them to

extrapolate the results to the full-scale. McCormick (1958) developed analytical expressions for predicting TVC inception at high Reynolds numbers. Kuiper (1981) and Arndt (1986) also carried out extensive investigations into the factors influencing inception of tip and trailing vortex cavitation.

Numerical methods are very valuable to assess the contribution of different source mechanisms to the underwater noise and to provide the required information for the development of propellers with low radiated sound level. Most of the methodologies applied in the field of hydroacoustic benefited greatly from the research activities in aeroacoustics field.

The hybrid method, which combines an incompressible hydrodynamic solver and the FWH (Ffowcs Williams Hawkings) acoustic analogy introduced by Ffowcs Williams & Hawkings (1969) is the most popular approach. The permeable FWH (P-FWH) developed by Di Francescantonio (1997) is also frequently used. Direct FWH, which is based on the 1A formulation developed by Farassat (2007), has been used successfully in various studies and application scenarios.

The aim of the present study is to develop an efficient control system to manage the acceleration of the RPS of the propeller in order to avoid cavitation and reduce the emitted non-cavitating noise of the propeller during the acceleration maneuvers. Based on the availability of the evaluation data, the geometry of the underwater vehicle test case DARPA (Defense Advanced Research Projects Agency) SUBOFF Groves (1989) and the propeller CNR-INM E1619 are selected. The numerical simulations are conducted using the RANSE solver STAR-CCM+ and the results are compared with those of the experiments carried out by Liu & Huang (1990). The hydrodynamic characteristics of the propeller used are calculated using the RANS method and the results are compared with experiment conducted by Yu-HsinLin (2023). Different flow simulations of acceleration maneuvers are performed for the SUBOFF configuration for the non-cavitating condition. In the maneuvers, different RPS increase scenarios are applied: abrupt, linear, parabolic, and using hyperbolic tangent function.

For the development of the control model for managing the acceleration maneuvers, the minimum pressure coefficient and the reduction of pressure on propeller blades due to increasing RPS are extracted from the simulation results by multivariable regression. Then, a mathematical model of pressure reduction and pressure fluctuation is developed to reduce noise radiation and to avoid cavitation inception.

In the final step of the study, a comparison is carried out between the noise emitted by the underwater vehicle investigated under different scenarios of acceleration and those when the developed control model is activated. The comparison is based on the results of the simulation performed using the hybrid CFD-PFWH method.

2 THEORITICAL ANALYSIS AND MATHEMATICAL MODEL

In the paper, an engineering method to predict TVC inception is applied. In addition, the Ffowcs Williams-Hawkings Equation is used to calculate the noise radiated from non-cavitating propeller. The hull of the SUBOFF with CNR-INM E1619 propeller is used to study the relation between TVC inception and different acceleration scenarios of the underwater vessel. The results are used to develop a simple control model for managing the RPS increase during the acceleration maneuver to avoid TVC inception and reduce non-cavitating noise.

2.1 TVC Inception

Tip vortex cavitation occurs when the pressure in the core of the vortex falls below the vapor pressure. The inception of TVC is a complex phenomenon that has been investigated by many researchers such as McCormick (1958), Kuiper (1981), Arndt (1991) and Chahine & Hsiao (2000). The TVC inception, can be detected using two different criteria. Firstly, by observation, as soon as elongated cavities form along the vortex axis, this is considered to be the beginning of TVC (Arndt et al. 1991). This method depends on the experience of persons involved and therefore does not provide accurate results. The second criterion is the acoustic inception which is used by Song (2016). The noise radiated from the propeller is monitored and TVC is considered to have begun when a certain number of noise events per time can be detected.

In the present study, a simple criterion is applied, namely that the minimum pressure must not fall below the vapor pressure (P_v), (Carlton 2007):

$$-c_P \geq \sigma_i \quad \textbf{(1)}$$

where σ_i is cavitation number of TVC inception.

$$\sigma_i = \frac{P_\infty - P_v}{{}^1\!/_2 \rho (nD)^2} \quad \textbf{(2)}$$

ρ, n and D are the fluid density, the number of revolutions, and the propeller diameter, respectively. P_∞ is the pressure in the flow field far from any disturbance considered at the same water depth of the evaluation point. The minimum pressure on the propeller blade P_{min} is used to calculate the minimum pressure coefficient c_P

$$c_P = \frac{P_{min} - P_\infty}{{}^1\!/_2 \rho (nD)^2} \quad \textbf{(3)}$$

2.2 Ffowcs Williams-Hawkings Equation

The current work is based on the FWH equation in the Farassat 1A formulation as described by Farassat (2007), which is:

$$p'(x, t) = P'_L(x, t) + P'_T(x, t) \quad \textbf{(4)}$$

Where p' is the sound pressure at observer position x and time t; P'_L *and* P'_T are called the loading and thickness terms respectively.

$$P'_T = \frac{1}{4\pi}\left(\int_{f=0} \left[\frac{\rho_0(\dot{U}_n + U_n)}{r(1-M_r)^2}\right] ds + \int_{f=0} \left[\frac{\rho_0 U_n \{r\dot{M}_r + c_0(M_r - M^2)\}}{r^2(1-M_r)^3}\right] ds\right) \quad \textbf{(5)}$$

$$U = v + \frac{\rho}{\rho_0}(u - v) \quad \textbf{(6)}$$

Where f = 0 denotes the integration surface for FWH equation; M is the vectorial Mach number, ρ_0 is the undisturbed fluid density, c_0 is the sound speed, u is the fluid speed, v is the surface moving velocity, and r is the vector from the source point to the observer position.

$$P_L' = \frac{1}{4\pi c_0}\left(\int_{f=0}\left[\frac{\dot{L}_r}{r(1-M_r)^2}\right]ds + \int_{f=0}\left[\frac{L_r\{r\dot{M}_r + c_0(M_r - M^2)\}}{r^2(1-M_r)^3}\right]ds\right) + \frac{1}{4\pi}\int_{f=0}\left[\frac{L_r - L_M}{r^2(1-M_r)^2}\right]ds \quad (7)$$

$$L = p\,n + \rho u(u_n + v_n) \quad (8)$$

Where n is the unit normal vector on the surface directing into the fluid domain, L_M = L.M and all variables are computed at the corresponding retarded times, that is, at τ = t- (r /c_0). The quadrupole component is ignored.

The position **r** changes between the sound generating time τ and the receiving time t due to the moving of the observer with regard to the static fluid. Brès et al. (2010) provided the formulae for calculating the vector r, that is,

$$r = \left(\frac{\Delta x + M_0\sqrt{\Delta x^2 + \beta^2(\Delta y^2 + \Delta z^2)}}{\beta^2}, \Delta y, \Delta z\right) \quad (9)$$

with

$$\beta = \sqrt{1 - {M_0}^2} \quad (10)$$

$$M_0 = \frac{u_0}{c_0} \quad (11)$$

Where Δx , Δy, Δz are components of the vector from the source point to the observer position at the time of sound generation, and u_0 is the observer's velocity along the x direction. These equations can be applied directly to P-FWH while another simplification can be achieved, when the formulation is applied to solid surfaces.

2.3 SUBOFF Geometry

As shown in Figure 1, the SUBOFF geometry investigated is an axisymmetric hull consisting of 4 main parts (bow forward part, middle part, stern part, stern cap). The hull has an overall length of 4.356 m and a maximum diameter of 0.508 m. The main particulars are given in Table 1.

Table 1 :Main dimensions of DARPA SUBOFF.

Overall length	4.356 m
Max diameter	0.508m
Forebody length	1.016m
Parallel mid-body length	2.229m
After body length	1.111m
Hull wetted area	6.338 m^2

Figure 1 shows the underwater vehicle with appendages and the coordinate system used. The trailing edges of the stern appendages are located at (4.007 m). The height of the rudders is 0.311m. The sail is located at x= 0.924 m and has a total length of 0.368 m.

Figure 1: DARPA SUBOFF with full appendages.

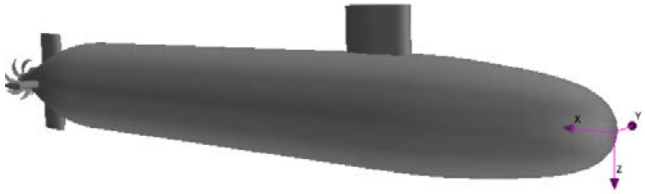

2.4 CNR-INM E1619 Propeller

As mentioned above, the 7-bladed CNR-INM E1619 is used in the present study. The main parameters of the propeller are shown in Table 2 and Figure 2.

Table 2: Main characteristics of CNR-INM E1619.

Diameter (D)	260.9 mm
Number of blades (Z)	7 blades
Hub diameter ratio (h_D/D)	0.23
Disc area ratio (A_0)	0.608

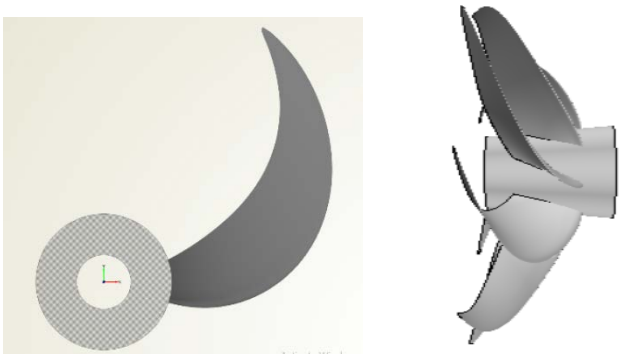

Figure 2: CNR-INM E1619 Propeller.

2.5 CFD Set-up

Figure 3 shows the dimensions of the computational domain, which are selected so that the blockage effect caused by the investigated hull of the submarine is less than 3 %, which corresponds to the recommendations given in (Ferziger & Peric 2002). The polyhedral cell mesher is applied as it is a reliable core mesher for external flow. A prism layer mesh is considered in the boundary layer region on the submarine. Refinement grid regions are defined around the hull, rudders and sail to reduce the discretization errors. A rotating domain is included to take the propeller rotation into account. The cell sizes in the different regions are shown in Table 3.

Table 3: Mesh size.

	Target surface size	Minimum surface size
Hull surface	0.03m	0.005m
Propeller mesh	0.004m	9e-4 m
Rotating domain mesh	0.01 m	0.005 m

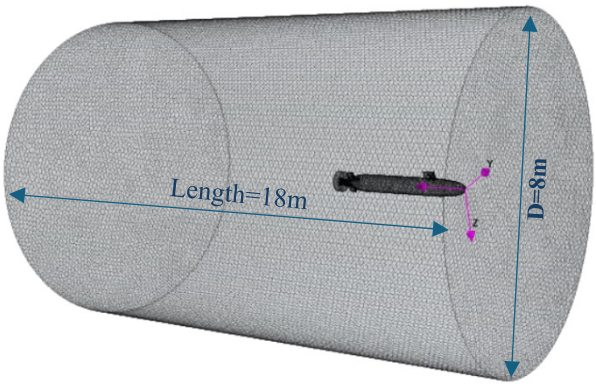

Figure 3: Computational domain

2.6 Acceleration Scenarios

All simulations begin with a steady state motion at 1.2 m/s straight ahead speed a number of revolutions of 15 RPS. This condition continues until 0.4 second, then the RPS starts to increase according to various scenarios.

As mentioned previously, three different scenarios of the increase in RPS are applied to define the relationship between the minimum pressure on propeller blades as a function of the actual RPS and its change rate as well as the vehicle acceleration. The simulation time is kept in all computation the same (10 seconds).

In the first scenario RPS increases instantly, while in the second scenario, the increase in RPS is linear with time and in the third scenario the RPS increase follows a hyperbolic tangent function over the time.

3 RESULTS AND DISCUSSION

3.1 Validation of the Set-up

The calculated total resistance values at different constant forward speeds are compared with those measured by Liu & Huang (1990). As shown in Table 4, the difference does not exceed 3%, which is considered to be acceptable for the present study.

Table 4: Results of total resistance.

Velocity (Knot)	Experiment Newton	CFD Newton	Difference in %
5.93	102.3	105	+2.5
16	675	689	+2.0
17.79	821	840	+2.3

Figure 4 shows a comparison of the calculated friction resistance coefficient with the values obtained by the ITTC formulas. As expected, the friction resistance coefficients decrease with increasing the speed. It can be seen, that there are some minor differences between the friction coefficients based on CFD results and ITTC and, the percentage of difference increases with the Reynolds number.

The reason for the increasing difference may be the change in pressure distribution around SUBOFF with increasing speed. This change is considered in the CFD calculations, but not in the ITTC formula. The percentage difference between them is less than 10%.

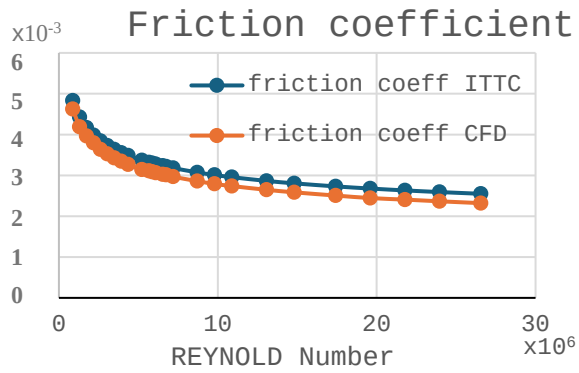

Figure 4: Friction coefficient at different Re numbers.

In addition, the results of the CFD-simulations of propeller open water test are compared with those of an experimental investigation conducted at the NCKU towing tank, (Yu-Hsin Lin 2023).

As shown in Table 5, the open water test is carried out at a constant number of revolutions per second (13 RPS) while the advanced velocity is changed.

Table 5: Experimental conditions of open water test (Yu-HsinLin 2023).

RPS (rev/s)	Va (advanced vel) m/s	Advanced Coeff. (J)
13	0.25	0.074
	0.75	0.221
	1.75	0.516
	2.25	0.663
	3.00	0.884

Table 6 includes the simulation and the measured results of the open water test. As it can be seen, good agreement with the experimental data has been achieved in general. However, the thrust and the torque predictions were underestimated at high advanced velocity.

Table 6: The comparison between experimental data and numerical result for open water test.

J	Kt (Exp)	Kt (CFD)	Error %	10Kq (Exp)	10Kq (CFD)	Error %
0.074	0.526	0.515	-2.0	0.733	0.750	2.3
0.221	0.481	0.476	-1.1	0.696	0.710	2.0
0.516	0.373	0.361	-3.2	0.607	.575	-5.0
0.663	0.308	0.295	-4.3	0.543	0.52	-4.0
0.884	0.195	0.181	-7.2	0.412	0.374	-9.0

3.2 Results of Different Acceleration Scenarios

In the three scenarios investigated, the submarine is accelerated in order to reach the same RPS target value, but different gradients of rotational speeds are employed. Figure 5 shows the change of minimum pressure on propeller blades by abrupt changes in RPS according to the first scenario. A sudden increase in RPS leads to a significant pressure reduction on the propeller blade. The pressure drops to a minimum value immediately, then returns to a certain minimum pressure value. In fact, minimum pressure on blades is affected not only by the number of revolutions but also by its rate. That sudden drop in minimum pressure has a considerable impact on the increase of the radiated noise. In addition, this drop may reach vapor pressure, which means cavitation inception of the tip vortex can take place.

Figure 6 shows that the strong reduction of the minimum pressure disappears in the second scenario (linear) when the instant change in RPS is avoided.

As shown in Figure 7, the scenario of hyperbolic tangent function acceleration shows not only less fluctuation in pressure than in linear acceleration case but also less time is needed to reach the same RPS, which is very advantageous for naval vessels.

To utilize this advantage, the control model developed for managing acceleration has been extended to allow the use of multiple hyperbolic tangent functions connected in series.

3.3 Regression Formulas

A regression analysis is conducted using the SPSS software package to define the relationship between the minimum pressure on the propeller blades, RPS, and speed of the submarine as well as the minimum pressure coefficient value on the SUBOFF hull. The regression formulas determined are validated using the results of new numerical simulations of different acceleration scenarios.

A linear equation and a second order equation are defined to describe the reduction of the minimum pressure on the propeller blade as a function of the RPS and the ship speed, see Equations (12) and (13) respectively.

$$P_{dy}(pascal) = -146117.4 + 10466 * n + 18827.6 * v \quad \textbf{(12)}$$

$$P_{dy}(pascal) = -27007.034 + 1484.317 * n + 12206.44 * v + 221.28 * n^2 + 8157.6 * v^2 - 1470.728 * n * v \quad \textbf{(13)}$$

The Equations (12) and (13) are verified using the CFD data of an acceleration maneuver and the results are compared in Figure (8).

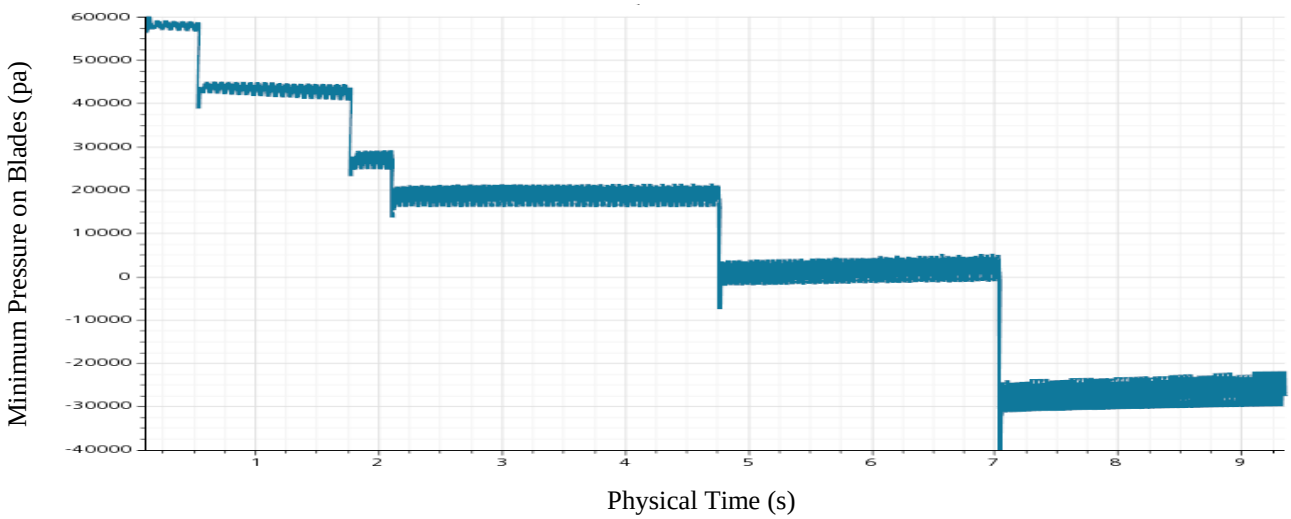

Figure 5: Minimum pressure on propeller in first scenario (at depth=0 m).

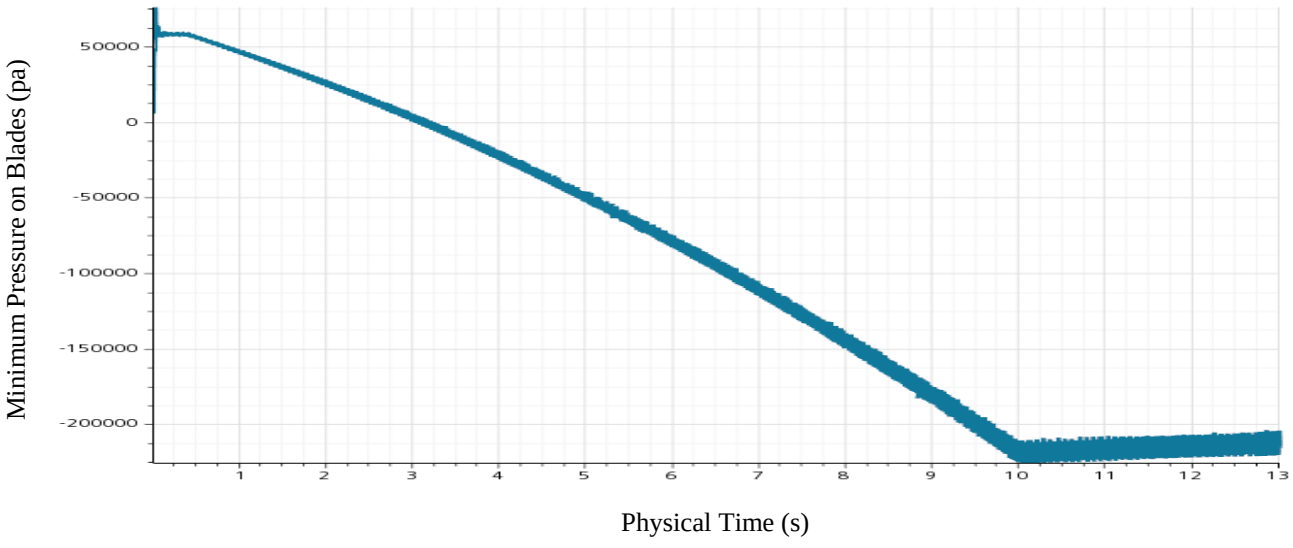

Figure 6: Minimum pressure on propeller in second scenario (at depth=0 m).

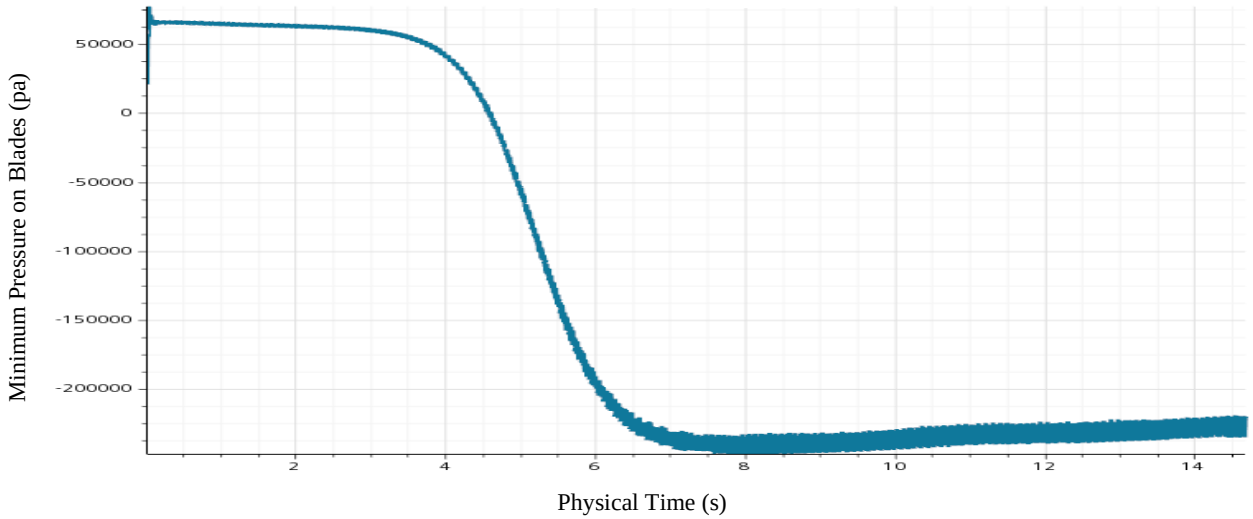

Figure 7: Minimum pressure on propeller in third scenario (at depth=0 m).

As it can be seen in Figure 8, the deviations between the results of the CFD simulation and those of the nonlinear equation are much less than the corresponding values of the linear equation. The mean deviation in the results of the nonlinear equation is less than 1.5%, but, the formula is still not able to not predict the fluctuation of pressure due to the sudden change of RPS.

The control model developed uses the minimum pressure coefficient for the determination of the maximum permissible acceleration of RPS. In the non-cavitating case, the minimum pressure coefficient is a constant value for the particular vessel under the same operation conditions such as distance from the free surface, water temperature, etc.

According to the nonlinear regression equation, the minimum pressure coefficient in the present study is 0.61. However, the influence of the sudden change of the RPS rate must be taken into account. As shown in the first scenario, the sudden increase in RPS causes an abrupt pressure drop, see Figure 5.

In the first scenario, the increase in RPS is conducted in a single-time step. This means that the rate of change in the RPS is:

$$\dot{n} = (n_{incr}) / (0.001) \quad \textbf{(14)}$$

Where $\dot{n}$ is the rate of change in RPS, 0.001 is the time step in the simulation and n_{incr} is the increment of number of revolutions.

In addition, the minimum pressure coefficient can be divided into a steady and an unsteady part as shown in Equation (15):

$$c_{p_{min}} = c_{p_{min\,at\ const\ n}} + c_{p_{min\,due\ to\ change\ in\ n}} \quad \textbf{(15)}$$

The minimum pressure coefficient due to the increment of RPS is proportional to the rate of change in RPS.

$$c_{p_{min\,due\ to\ change\ in\ n}} \propto \dot{n} \quad \textbf{(16)}$$

$$c_{p_{min\,due\ to\ change\ in\ n}} = const * \dot{n} \quad \textbf{(17)}$$

The analysis of the outputs of various simulations shows that a constant value of 0.0001 provides results that are very close to those of the simulation.

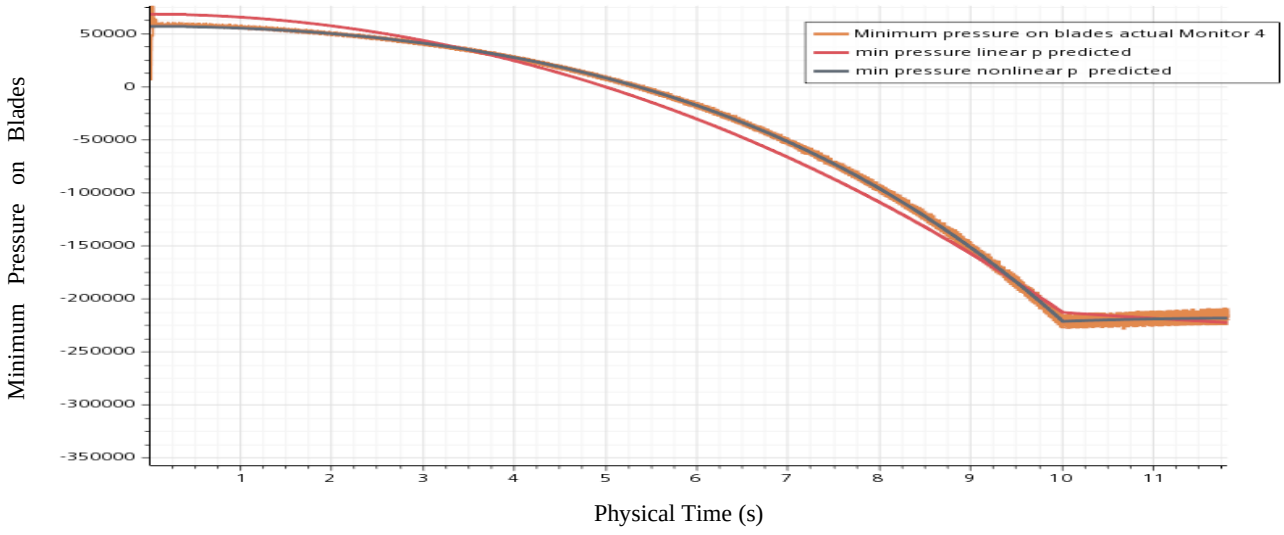

Figure 8: Comparison between minimum pressure on blades and estimations of different regression equations.

Although the constant value is small, it is absolutely needed to calculate the minimum pressure coefficients for an abrupt increase in the RPS rate. The Equation (17) is considered only when $\dot{n}$ exceeds a certain limit.

3.4 Controlled Acceleration Model

The model must be able to estimate the cavitation inception as a function of the operation conditions, such as the operating depth of SUBOFF, water temperature, the actual and the demanded RPS. These input parameters are required to determine the hydrostatic pressure on blades, vapor pressure, and maximum allowable increment of the RPS respectively. Then, the model calculates the highest possible RPS increment rate and automatically builds the function for control the increasing of the RPS. Figure 9 shows the flow chart of the system developed to fulfil this specific requirement.

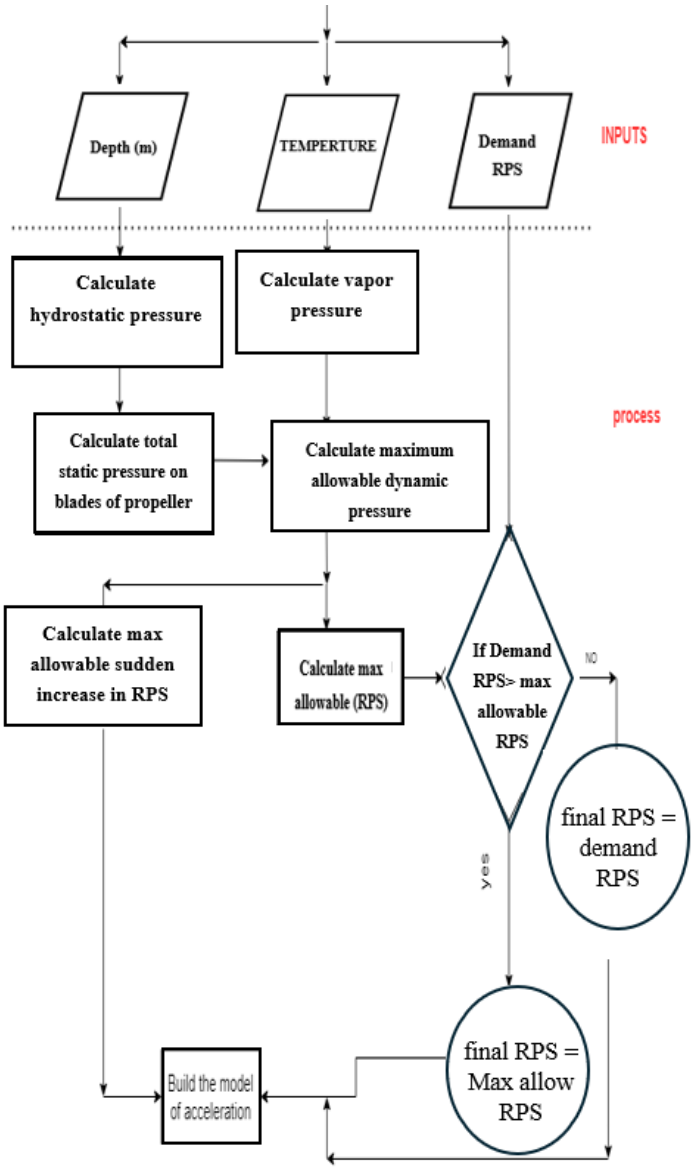

Figure 9: The flow chart of control system.

The vapor pressure P_v is calculated using a simple formula that depends only on the temperature of the water given by Carlton (2007) as shown in Equation (18)

$$P_v(mmHg) = e^{(20.386-\left(\frac{5132}{temp(kelvin)}\right))} \quad \textbf{(18)}$$

The achievable RPS (n_{final}) at the end of acceleration is dependent on both maximum allowable RPS (n_{allow}) to avoid cavitation and demanded RPS ($n_{demanded}$)which is specified in accordance with the operating situation.

n_{allow} is dependent on the total hydrostatic pressure $P_{total\ hydrostatic}$ and the minimum pressure coefficient $c_{p_{min}}$ on the blade, which is extracted using Equations (19) and (20):

$$c_{p_{min}} = \frac{P_{dy_{\max allow}}}{0.5\rho((\pi nD)^2+v_a{}^2)} \quad \textbf{(19)}$$

Where v_a is the vehicle speed. Due to the high value of the RPS in the investigated cases, the contribution of v_a to the total speed is too small, therefore, the vehicle speed can be neglected in the Equation (19). The maximum allowable RPS to avoid cavitation n_{allow} can be calculated as follows:

$$n_{\max allow} = \sqrt{\frac{P_{dy_{\max allow}}}{2\rho c_{p_{min}}\pi^2 r^2}} \quad \textbf{(20)}$$

$$P_{dy_{\max allow}} = P_{total\ hydrostatic} - P_v \quad \textbf{(21)}$$

$P_{total\ hydrostatic}$ is the total hydrostatic pressure it includes the atmospheric and the hydrostatic parts. The model developed checks the allowable instant increase in RPS to avoid cavitation inception based on the Equation (17), which is used to describe the pressure reduction due to an instant increase in RPS.

3.5 Results of the Controlled Model

Various tests were carried out to evaluate the functionality of the control model. It has been assumed that the water temperature is 25 degrees. The model operates 5 meters below the water-free surface. The start and the demand RPS are 15 and 30, respectively. Then, the control model starts the calculation of the vapor pressure using Equation (18), the maximum allowable RPS using Equation (19). The calculated vapor pressure is 3156 Pa, while the maximum allowable RPS is 25, the demand RPS is higher than the maximum allowable RPS. Therefore, the system chooses different strategy to achieve the final RPS. The increase of the RPS in conducted in three phases. In the first phase, a maximum allowable sudden increase of 2 rev/sec is allowed. According to Equation (17) the change in minimum pressure coefficient is equal to 0.20. Finally, the control system uses two hyperbolic tangent functions for control the acceleration. The variation of the RPS over time is shown in Figure 10.

The results show that during the acceleration cavitation inception is avoided as the minimum pressure on the propeller blades is always higher than the vapor pressure, see Figure 11.

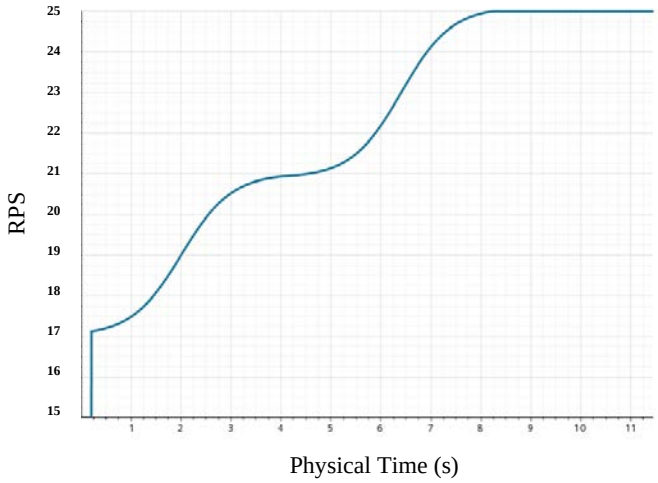

Figure 10: change of RPS in control model.

However, the increase in non-cavitating noise is limited but still present.

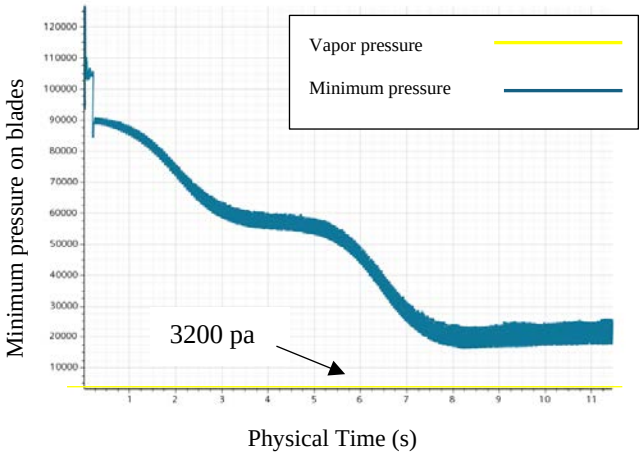

Figure 11: Minimum pressure on blades(absolute) during acceleration.

In the next section, the non-cavitating noise occurs when various acceleration scenarios are applied.

3. 6 Non-Cavitating Noise for Different Scenarios

The radiated sound pressure from the propeller is calculated for the three different scenarios using the P-FWH implemented in STAR-CCM+. Four receivers at different positions are considered, see Figure12 and Table 7. The sound pressure decreases with time, as the distance between the fixed receivers and the moving vehicle increases.

Table 7: location of noise observer.

	Location in meter
Receiver 1	[4.35, 0, 5]
Receiver 2	[4.35, 0, 1]
Receiver 3	[4.35, 0, -1]
Receiver 4	[5.35, 0.0, 0.0]

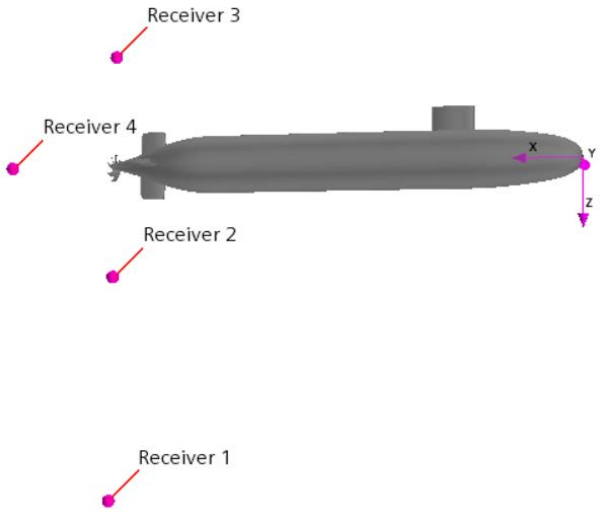

Figure 12: location of noise observer to SUB OFF.

As mentioned, non-cavitating noise does not depend only on the minimum pressure on the blade but also on the distribution of the pressure on the blade as well as the difference in pressure between the suction side and pressure side. Figure 13 (a and b) shows the pressure distribution on the suction and pressure side of the propeller, respectively, for the first scenario (sudden change in RPS). The low-pressure areas are significantly larger than those in the linear acceleration scenario shown in Figure 13(c and d), respectively. Therefore, it should be expected that the sound level generated due to the pressure distribution in the first scenario is much higher than the sound level generated in the second (linear) scenario. Figure 13 (e and f) shows the pressure distribution on the propeller blades, when the rate of change of the RPS is changed from the linear to the minimum pressure-controlled scenario according to the hyperbolic tangent function.

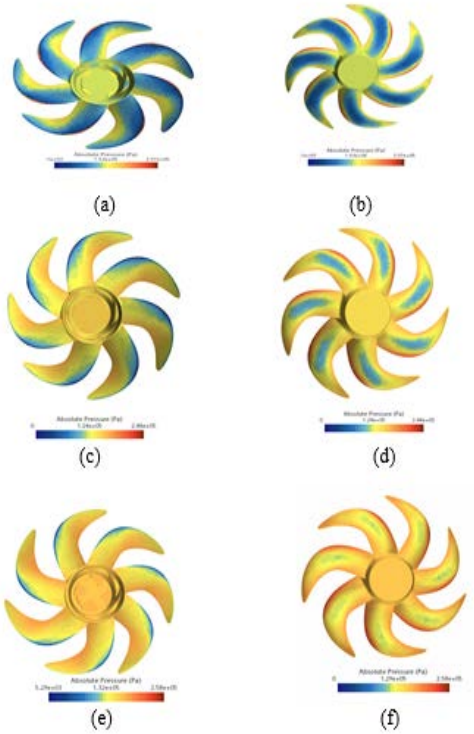

Figure 13: Pressure distribution on propeller blades during different simulation.

It can be seen that the low-pressure area on the suction side being reduced and almost disappearing on the pressure side, meaning that the radiated noise of the controlled scenario is lower than in the linear acceleration one. As shown in Figure 14, the first scenario with a sudden increase shows maximum sound pressure peaks at all receivers. These peaks are due to the sudden pressure drop caused by the abrupt increase in RPS. The range of sound pressure amplitudes is larger than that in other two scenarios. The second scenario with linear acceleration shows a range of sound pressure higher than the third scenario. This confirms that controlled acceleration is the appropriate way to increase the number of revolution while keeping non-cavitating noise to a minimum.

analyze the relationship between RPS and the minimum pressure on the propeller blades.

As expected, with increasing RPS, the minimum pressure on propeller blades reduces. In addition, a sudden increase in the RPS results in the abrupt drop of pressure.

A regression method is applied to analyzing the simulation data and correlating a relationship between the minimum pressure on the propeller blades, RPS, and the speed of underwater vehicle. A linear and nonlinear relations are determined and verified.

The results of the nonlinear equation show a good agreement with the resultant minimum pressure on the propeller blade using the CFD simulations, the mean deviation is about 1.5%.

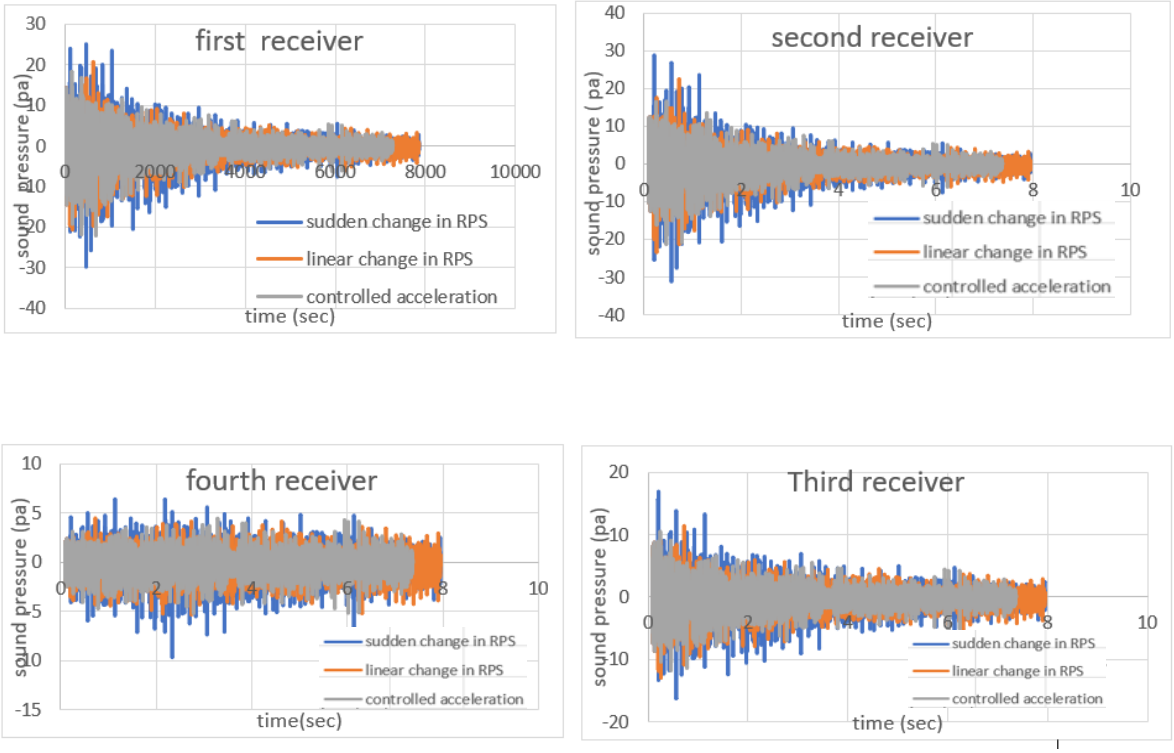

Figure 14: Sound pressure radiated from different scenarios.

4 CONCLUSIONS

A simple control model for the acceleration of the propeller of an underwater vehicle was developed. This model aims to reduce the radiated noise from the propeller besides avoiding tip vortex cavitation. The developed model allows fast and accurate analysis of the pressure reduction on the propeller blades and is able to predict the tip vortex cavitation inception. For validation purposes, the total resistance of the investigated underwater vehicle is validated against the published experimental results. In addition, the friction resistance coefficient obtained via the CFD simulations is compared with the corresponding value calculated by the friction resistance formulae of (ITTC 1957). An overall good agreement is observed. Furthermore, the results of the open water test simulation show a good agreement with the experiment.

Three different scenarios for increasing the RPS (abrupt, linear and minimum pressure controlled) are applied to

The control of underwater vehicle acceleration maneuver is based on a model for managing the temporal increase of the RPS. The model must be able to consider the influence of the related operation conditions such as distance to the free surface, the water temperature, the actual and the demanded RPS. The controlled acceleration model follows hyperbolic tangent functions for the change in RPS, which can be adjusted and connected in series. Also, a sudden increase in RPS at the beginning of the acceleration allowed in order to shorten the time required to reach the full RPS demand. In addition, the control system calculates the permissible acceleration to avoid cavitation phenomena, whereby the minimum pressure at the propeller blades is always kept above the vapor pressure.

Finally, the hybrid method, which combines CFD and PFWH is used to calculate the acoustics pressure and estimate the radiated noise from the propeller. The non-cavitating noise emitted when using the controlled

acceleration model was compared with the noise emitted in the other two scenarios - abrupt and linear change of RPS. The noise emitted when the control model is activated is significantly lower than in the other scenarios.

This developed model can be adapted to any underwater vehicle and propeller configuration. However, CFD simulations must be carried out to calculate the minimum pressure coefficient on the propeller blade surface as a function of the RPS rate.

ACKNOWLEDGEMENTS

The numerical calculations were conducted on the HPC system in Maritime Technology Studies Institute. A special thanks go to Dr.-Ing. Jan Clemens Neitzel-Petersen, Hamburg University of Technology for his great efforts especially by developing the CFD setup. The authors are grateful to Dr. Mario Felli (Institute of Marine Engineering (INM) National Research Council (CNR)) for providing the propeller geometry.

REFERENCES

Arndt, R. E. A., Arakeri, V. H., & Higuchi, H. (1991). 'Some observations of tip-vortex cavitation'. Journal of Fluid Mechanics, vol 229, pp. 26S289.

Asnaghi, A., Svennberg, U., & Bensow, R. E. (2018a). 'Numerical and experimental analysis of cavitation inception behavior for high-skewed low-noise propellers. Applied Ocean Research, vol 167, pp150-162.

Asnaghi, A., Svennberg, U., & Bensow, R. E. (2018b). 'Analysis of tip vortex inception prediction methods', Applied Ocean Research, vol 167, pp187-203.

Bres, G.; Pérot, F.; Freed, D. A Ffowcs Williams-Hawkings solver for Lattice-Boltzmann based computational aeroacoustics. In Proceedings of the 16th AIAA/CEAS Aeroacoustics Conference, Stockholm, Sweden, 7–9 June 2010; p. 3711.

Carlton,J. (2007). Marine Propellers and Propulsion. 2nd ed. Butterworth-Heinemann Book Company.

Di Francescantonio., P. (1997). 'A new boundary integral formulation for the prediction of sound radiation.', In Journal of sound and Vibration (Vol. 202, Issue 4).

Farassat, F. (2007). 'Derivation of Formulations 1 and 1A of Farassat'. Technical Report NASA/TM-2007-214853; NASA, Langley Research Center: Hampton, VA, USA, 2007.

Ferziger, J. H., & Peric, M. (2002). Computational Methods for Fluid Dynamics.3rd edition. Stanford, springer.

Ffowcs Williams, J. E., & Hawkings, D. L. (1969). 'Sound Generation by Turbulence and Surfaces in Arbitrary Motion'. Series A, Mathematical and Physical Sciences (Vol. 264, Issue 1151).

Franc, J.-P.,&Michel, J.-M. (2003). 'Fundamental of Cavitation'. Grenoble Science, Springer press.

Groves, Nancy. (1989). 'Geometric Characteristics of DARPA SUBOFF models. DTRC/SHD, USA.

Kuiper, G., 1981. 'Cavitation Inception on Ship Propeller Models'. PhD-thesis. Delft. University of Technology.

Liu, H.-L., & Huang, T. T. (1990). 'Summary of DARPA SUBOFF Experimental Program Data'. DARPA Task Area, USA.

Wang, Y., Göttsche, U., Abdel-Maksoud, M. (2020). 'Sound Field Properties of Non-Cavitating Marine Propellers'. J. Marine Science and Eng., 8, 885.

Yu-Hsin Lin & Ahmad Darori Hasan1 (2023). 'The CFD simulation of E1619 propeller open-water tests validated by the EFD in the NCKU towing tank'. Journal of Mechanics, vol 39, pp416-430.

Song J, Kim J (2016). 'Measurement of temperature effects on cavitation in a turbopump inducer'. Journal of Fluids Engineering, vol 138, pp170-180